Ann. Geophys., 26, 3113–3125, 2008
www.ann-geophys.net/26/3113/2008/

Annales Geophysicae

A review of the quantitative links between CMEs and magnetic clouds

P. Démoulin

Observatoire de Paris, section de Meudon, LESIA, UMR 8109 (CNRS), 92195 Meudon Cedex, France

Received: 7 September 2007 – Revised: 13 November 2007 – Accepted: 15 November 2007 – Published: 15 October 2008

Abstract. Magnetic clouds (MCs), and more generally, interplanetary coronal mass ejections (ICMEs), are believed to be the interplanetary counterparts of CMEs. The link has usually been shown by taking into account the CME launch position on the Sun, the expected time delay and by comparing the orientation of the coronal and interplanetary magnetic field. Making such a link more quantitative is challenging since it requires a relation between very different kinds of magnetic field measurements: (i) photospheric magnetic maps, which are observed from a distant vantage point (remote sensing) and (ii) in-situ measurements of MCs, which provide precise, directly measured, magnetic field data merely from one-dimensional linear samples. The association between events in these different domains can be made using adequate coronal and MC models. Then, global quantities like magnetic fluxes and helicity can be derived and compared. This review paper describes all the general trends found in the above association criteria. A special focus is given for the cases which do not follow the earlier derived mean laws since interesting physics is usually involved.

Keywords. Interplanetary physics (Interplanetary magnetic fields) – Solar physics, astrophysics and astronomy (Flares and mass ejections)

1 Introduction

Coronal mass ejections (CMEs) expel plasma and the magnetic field from the Sun into the interplanetary medium, where the observed structures are called interplanetary CMEs (ICMEs). A subset of these ICMEs, known as magnetic clouds (MCs), is characterized by enhanced magnetic field strength with respect to ambient values, a smooth and large rotation of the magnetic field vector, and low proton temperature (e.g. Burlaga, 1995).

The derivation of the ICME physical properties from the observations of the associated CME is vital for any prediction of the geophysical effectiveness, and therefore for space weather forecast. However, before achieving this goal, we have to understand precisely how a given CME, with some observed coronal characteristics, evolves into the interplanetary medium. An MC is plausibly observed only when the spacecraft crosses the central part of an ICME (Jian et al., 2006). Since MCs have more clearly defined physical characteristics, than non-MC ICMEs, the association can be stronger using more physical quantities. Below,"MC" is used only when the presence of a flux rope is required, while "ICME" is generically used otherwise.

The magnetic field has a key role in CMEs and ICMEs (low β plasma). However, we have only indirect information on the coronal magnetic field (mainly from magnetic extrapolations of photospheric magnetograms and from coronal loop observations). On the other hand, we have precise measurements of the vector magnetic field in the interplanetary medium. The limitation here is rather the localize nature of the measurements (available only along a line as the ICME overtakes the spacecraft). We can take advantage of this situation by relating a CME to its associated ICME every time data are available in both domains. Then, we can benefit from the strength of the measurements in both domains.

The association of CMEs to MCs/ICMEs is certainly a main way to understand these phenomena, but also to be able to predict their effect on the magnetosphere. Significant progresses has been made in finding this association (Sect. 2–5). Global quantities, magnetic fluxes and helicity have been compared (Sects. 6 and 7).

Correspondence to: P. Démoulin
(pascal.demoulin@obspm.fr)

Published by Copernicus Publications on behalf of the European Geosciences Union.

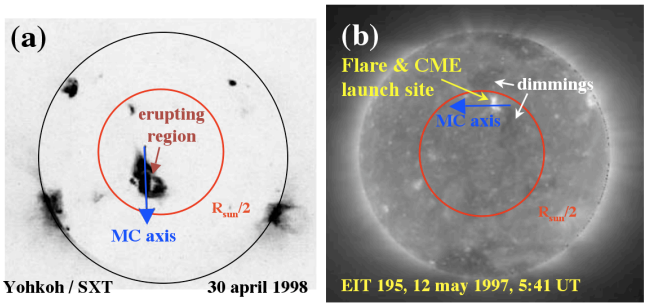

Fig. 1. Examples of eruptions located close to the solar disk center and with an associated MC detected in the Earth vicinity. The images are taken: **(a)** in X-rays (Watari et al., 2001), and **(b)** in EUV (Webb et al., 2000). The blue arrow indicates the MC axis deduced at 1 AU from in-situ data (see Fig. 5 for the definition of the MC axis). Other aspects of the event (b) are also shown in Figs. 7 and 12.

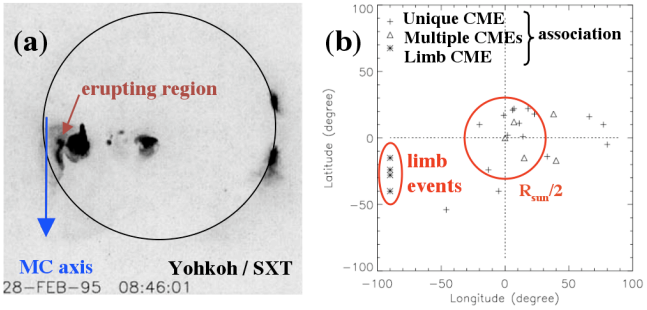

Fig. 2. Examples of MCs/ICMEs reaching the Earth while their source regions are located far from the solar disk center. **(a)** Eruption observed in X-rays (Watari et al., 2001). **(b)** Distribution of the source regions of CMEs causing major geomagnetic storms (Zhang et al., 2003). There is a global western asymmetry shift (comparable to the source location of the solar wind at Earth due to the Parker spiral). Still, four cases are coming from behind the eastern limb (thus with no visible solar source).

2 Location on the Sun

CMEs observed by coronagraphs above the solar limb have typically a radial motion at distances larger than several solar radii ($R_\odot$). Moreover, in-situ measurements also give a plasma velocity close to the radial direction. Then, when an ICME is observed in the vicinity of the Earth, its associated CME is expected to be a halo CME, or at least a partial-halo CME, and its source region is expected to be close to the disk center, say, closer than $R_\odot/2$ (Fig. 1). This extension of the source region takes into account the average angular size of CMEs (≈50°, St. Cyr et al., 2000).

However, there are exceptions, as shown in Fig. 2, with extreme cases having a launch site at the limb, or even behind! Zhang et al. (2003) found that the proportion of these extreme cases is especially large in the restricted class of

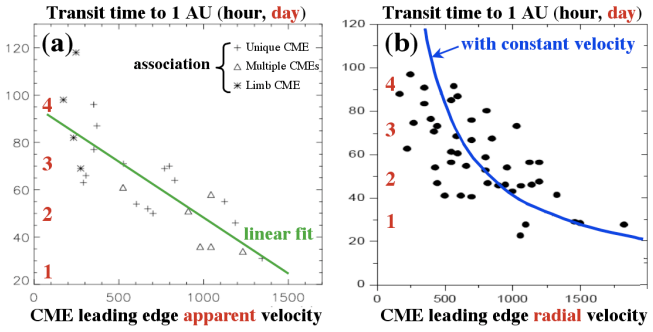

Fig. 3. The transit time of CMEs from the Sun to 1 AU as a function of their coronal velocity. **(a)** The abscissa is the leading edge velocity of halo CMEs observed by LASCO, so it is the velocity projected on the plane of sky (Zhang et al., 2003). **(b)** The abscissa is the radial velocity, $V_{\rm rad}$, measured from Helios 1 which was in quadrature with the Earth (within ±30°; Schwenn et al., 2005). The timing was corrected from Helios 1 to 1 AU by assuming a constant velocity. The comparison of the data to a model with constant velocity (curve) shows that ICMEs with a low initial coronal velocity are accelerated while fast ones are decelerated. The results of the two panels can be related to the result of Schwenn et al. (2005) on limb CMEs observed by LASCO: $V_{\rm rad}$≈$0.88V_{\rm exp}$ (where $V_{\rm exp}$ is the full lateral expansion velocity of the leading edge).

ICMEs leading to major geomagnetic storms (this implies a further difficulty in predicting the most geo-effective ICMEs from solar data). Indeed, some CMEs are very large scale, involving half of the solar corona, so in these cases the source regions can be far from disk center (Zhukov and Veselovsky, 2007). Also, CMEs do not always have a radial motion, but they can be deflected by streamers (e.g. Gopalswamy et al., 2000). Then, when searching for the ICME source region, the research can start close to the disk center but should not be limited to it.

3 Timing between the Sun and in-situ measurements

Starting from an observed eruption, the ICME counterpart can be searched through in-situ data at 1 AU in a time interval of 1 to 5 days after the eruption (corresponding to a mean transit velocity between 350 and 1800 km s^{-1}), with the exception of extreme events, like in October 2003, which reached the Earth in less than one day. The search can be simplified by taking into account the correlation found between the transit time and the CME velocity measured close to the outward edge of the coronagraph field of view (Gopalswamy et al., 2000, 2001; Zhang et al., 2003, Fig. 3). Schwenn et al. (2005) have shown that the leading edge expansion velocity (measured in the direction orthogonal to the main expansion direction) gives a better proxy to the radial velocity, as well as to the transit time, than the velocity measured in the direction of the largest expansion. Indeed, this last velocity is

in general a combination of the expansion and radial velocity with a projection on the plane of sky. Such a projection effect is not removed well enough using a cone model for the CME (Gopalswamy et al., 2001), while improvements have been achieved with developments on the cone model (Michałek et al., 2004).

Starting from an observed ICME, the eruption counterpart can be searched through solar data using the in situ averaged measured velocity in the ICME. The window time interval can be estimated, for each studied case, from the maximum and minimum plasma velocity (e.g. $V_{\rm ICME}$=450±50 km s^{-1} gives an expected eruption of 3.6±0.4 days earlier; Bothmer and Schwenn, 1998). A larger fixed time interval has also been used (e.g. ±1 day, Marubashi, 1997; Watari et al., 2001). The travel time estimation is usually more precise when starting from the interplanetary data than from the solar eruption for the following reasons. Firstly, a precise radial velocity is in-situ available; secondly, this measured velocity is closer to the mean velocity during the travel time since the deceleration (or acceleration) of the ICME is predominantly present close to the Sun (see Sect. 4); and finally, the global motion of the ICME is available (while at the Sun the leading edge velocity is the combination of the global and expansion motion).

Interplanetary type II radio bursts are observed usually only for some fast ICMEs, and the association is done by following the drift in frequency of the radio emission (Reiner et al., 1998; Berdichevsky et al., 2002). So far, this direct association can be realized only in a few cases. With an heliospheric density model, and assuming the type II emission to be radiated at the fundamental or second harmonic of the local plasma frequency (which varies as the square root of the plasma density), the radio frequency can be converted to a radial distance, so radio observations have the potential to monitor the velocity of the ICME from a few $R_\odot$ to the Earth and beyond. Since the solar-wind plasma density decreases almost as the inverse of the distance squared, the inverse of the radio frequency, $1/f$, varies as the distance. Then, in dynamic spectra plotted as a $1/f$ function of time, a uniform velocity is traced out by drifting emission features located along straight lines (Reiner et al., 1998; Hoang et al., 2007). The main limitations of the type II diagnostic is the patchy structure and the relatively large bandwidth of the emission (corresponding to variable plasma density and/or distance to the Sun). From 42 cases, Reiner et al. (2007) deduced that a nearly constant velocity is present only in the last part of the interplanetary travel to the Earth, while a deceleration occurs closer to the Sun. Within the model framework of a constant deceleration close to the Sun and uniform velocity later on, they conclude that the faster ICMEs decelerate stronger and more rapidly near the Sun. From other cases (e.g. Hoang et al., 2007), some ICMEs are found to accelerate near the Sun to a constant propagation speed later on in the interplanetary medium.

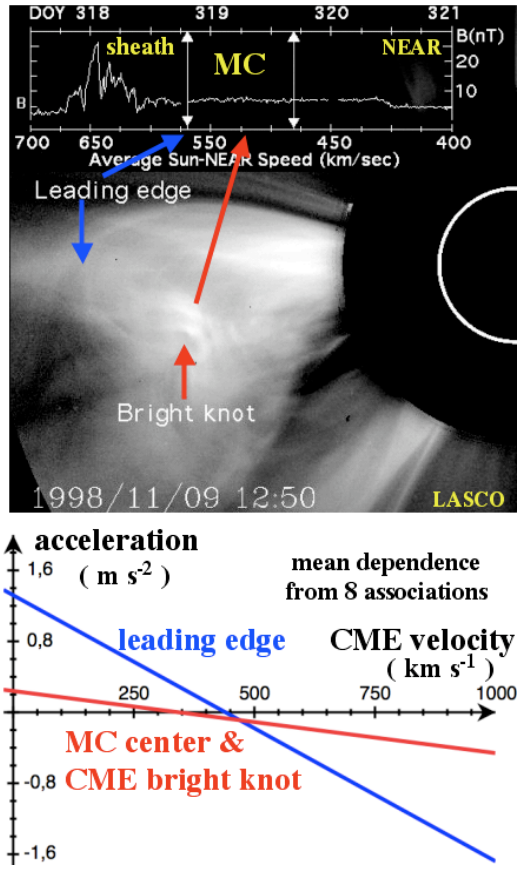

Fig. 4. Acceleration of MCs from observations in quadrature. The top panel shows a limb CME observed by LASCO with the associated in-situ measurements of the magnetic field strength by the NEAR spacecraft added on the top part. The abscissa is the arrival time (in days, upper axis); the corresponding mean transit velocity is reported on the lower horizontal axis. From the mean velocity, the radial velocity measured with LASCO and the transit time, a mean acceleration is computed. The least-squares fit of a straight line to the data results of 8 associations is shown in the bottom panel (Rust et al., 2005).

4 Observations in quadrature

When a CME is ejected toward the Earth, it is observed as a halo CME. This is not a favorable configuration to measure the escaping velocity from the Sun (mostly radial) with an observatory in the vicinity of the Earth.

The best configuration to study the dynamics of ICMEs is when the coronagraph and the in-situ observations are in quadrature, so that the CME is observed in the plane of the sky from the coronagraph point of view (Burlaga et al., 1982; Weiss et al., 1996). The leading edge of the CME is usually associated with the front of the associated ICME. CMEs observed below the average slow solar wind velocity (≈400 km s^{-1}) are typically accelerated, while those above this velocity are decelerated (Lindsay et al., 1999;

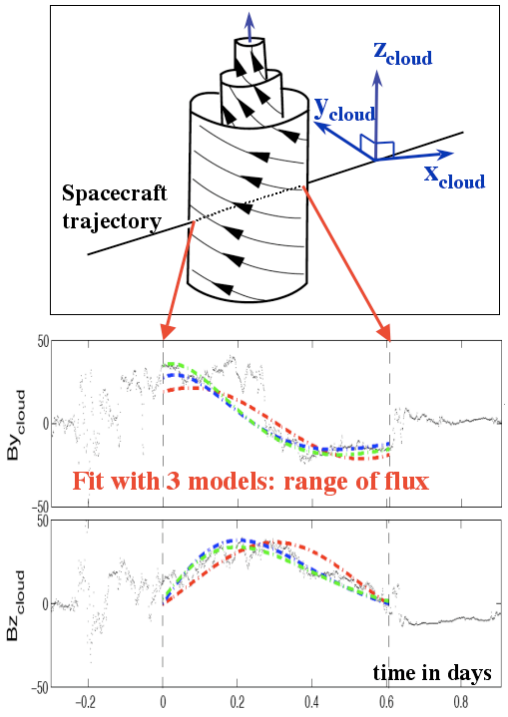

Fig. 5. Flux rope schema (top panel) and typical observed magnetic field components of a MC when rotated in the cloud frame (dots in the two lower panels). $\hat{z}_{\rm cloud}$ is along the cloud axis, $\hat{y}_{\rm cloud}$ is orthogonal to both the MC axis and the spacecraft trajectory, and $\hat{x}_{\rm cloud}$ completes the right-hand orthogonal base. The observed magnetic field in MCs usually has the characteristics of a flux rope. The signatures are a coherent reversal of $By_{\rm cloud}$ ($\approx$ azimuthal component), a peaked $Bz_{\rm cloud}$ (axial component), and a small $Bx_{\rm cloud}$ (not shown since it is globally constant and weak, due to a low impact parameter). The blue, green and red dashed curves are the fit using three flux-rope models (Mandrini et al., 2007).

Schwenn et al., 2005, Fig. 3). This result is classically interpreted as the result of the drag force between the ICME and the solar wind. The mean acceleration was derived by Gopalswamy et al. (2001) with observations between 0.6 and 0.9 AU and by Rust et al. (2005) with observations between 1.2 and 1.8 AU. The least-squares fit to the data gives an average acceleration from the Sun to the spacecraft (in $\mathrm{m\,s^{-2}}$) of: a=2.193−0.0054 u and a=1.32−0.003 u, respectively (where u is the leading edge velocity of the CME in $\mathrm{km\,s^{-1}}$). The difference of about a factor of 2 between these two results is likely to come from the factor $\approx$2 present in the distance of the spacecraft from the Sun and an acceleration mainly concentrated close to the Sun (dilution effect on the average).

The observations in quadrature also permit one to detect the bright core frequently present in the center of the limb CMEs. Rust et al. (2005) found an acceleration typically smaller by a factor of $\approx$4 for the center than the leading edge (Fig. 4). This implies that, in the studied MCs, the dynamics is mainly in the expansion of the magnetic structure (relative to its center). This result is in agreement with the analysis of two cases observed by Ulysses at a larger distance from the Sun ($\approx$4.6 AU). Funsten et al. (1999) found that the mean velocity of the center (computed from the transit time) was much closer to the in-situ measured velocity while the leading edge was significantly faster.

5 Orientation of the magnetic configuration

In the corona, the orientation of the erupting magnetic configuration is directly observable (magnetograms, filaments, coronal loops). In the interplanetary medium, the flux rope orientation needs to be deduced from the 1-D data using some assumptions. If the spacecraft is passing close enough to the flux rope axis (low impact parameter), one takes advantage of the different spatial variations of the field components to find the flux rope axis, using a minimum variance analysis (Bothmer and Schwenn, 1998; Gulisano et al., 2007): the axial direction, $z_{\rm cloud}$, corresponds to the eigenvector having the intermediate variance (Fig. 5). Improvements on the orientation can be realized by fitting flux rope models to the data. The comparison between various models gives an estimation of the uncertainty of the orientation (typically $\pm 10°$, see Dasso et al., 2005, for a review).

The direction of the MC axis was found to be roughly aligned with the disappearing filament (Bothmer and Schwenn, 1994, 1998). This result was quantified by Marubashi (1997) and Zhao and Hoeksema (1998) on ten cases, and by Yurchyshyn et al. (2001, 2005) and Ruzmaikin et al. (2003) on individual cases (Fig. 6). The MC axis is also often aligned with the corresponding X-ray sigmoid (Watari et al., 2001, Figs. 1, 2)

However, some MCs do show a significant rotation of their axis compared to their associated filament. One case is already present in the study of Bothmer and Schwenn (1994). Rotations larger than 30° are indeed not unusual: 5 out of 9 cases (Marubashi, 1997) and 2 out of 14 cases (Zhao and Hoeksema, 1998, Fig. 6). Such a rotation is also required in 11 out of 34 cases of CMEs (with 5 cases having a rotation larger than 70°), in order to best fit a flux rope model, with a shell of plasma density to the LASCO data of CMEs (Thernisien et al., 2006). An estimation of the rotation will also be available from the elliptic cone model of CMEs with the constraint of observations from two points of view (Zhao, 2007).

Green et al. (2007) analyzed in detail 7 associations of filament/MC having a large rotation. They found that the direction of the rotation is related to the sign of the magnetic helicity:

$$\mathrm{sign(rotation)}\ .\ \mathrm{sign(helicity)} > 0\,, \qquad (1)$$

where the rotation is counted positively in the clockwise direction from the filament to the MC axis direction (Fig. 7).

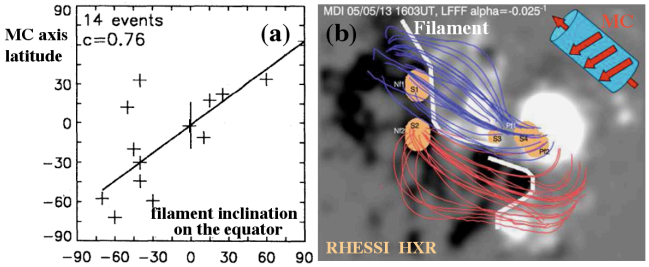

Fig. 6. Observed cases where the erupting filament and the associated MC axis have a comparable orientation. **(a)** Scatter plot and linear least-squares fits for 14 events. There is a relatively good correlation between the orientation of the filament and the MC axis, but they differ by more than 40° for the two events (Zhao and Hoeksema, 1998). **(b)** Example of association between an erupting filament and its related MC. Some field lines computed with a linear force-free extrapolation (blue and red lines) and the observed hard X-ray sources (pink regions) are added on top of the photospheric magnetogram (Yurchyshyn et al., 2006).

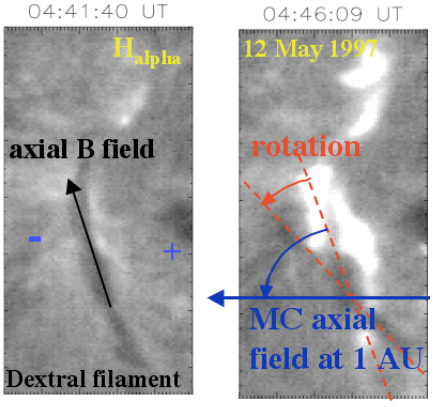

Fig. 7. Counterclockwise rotation of an erupting filament on 12 May 1997 (same event as shown on the left panel of Fig. 12). The magnetic configuration has a negative magnetic helicity, as shown by several indicators (see Fig. 16): the dextral filament, the relative shift of flare ribbons, and the associated reverse-S sigmoid observed in X-rays (not shown). The rotation is confirmed by the axis direction of the associated MC at 1 AU (Green et al., 2007).

This rotation is interpreted as the consequence of the writhing of the magnetic flux tube. Re-analyzing the results of Marubashi (1997), Eq. (1) is satisfied for 4 cases, while incorrect for 1 case (the other 4 cases have a rotation below 30°).

Magnetohydrodynamics simulations have shown that a moderate writhing of the twisted flux tube is already present in the equilibrium configuration (Török and Kliem, 2003; Aulanier et al., 2005). However, the writhing becomes large only when the kink instability sets in (Gibson et al., 2004; Török and Kliem, 2005, Fig. 8). With this twisted configuration, Eq. (1) is a natural consequence of the transfer of

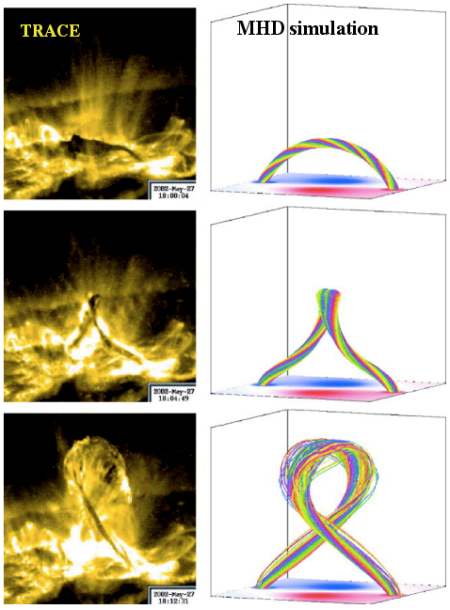

Fig. 8. Left panels: observations of a filament eruption close to the limb. Right panels: Magnetohydrodynamics simulation of the kink instability in a bipolar magnetic configuration. The simulation was rotated so that the photospheric magnetic inversion line corresponds to the initial direction of the observed filament. The simulated flux rope length was also scaled to the filament extension. The time evolution of the kinked flux rope is closely comparable to the observed filament writhing. Here the eruption is confined (thus better visible because it is denser). Similar results are also obtained in some eruptive cases (Török and Kliem, 2005).

magnetic helicity from the twist to the writhe in the flux tube.

Finally, the dispersion of observed rotation values is intriguing: some filament/MC axis are well aligned, while others show a significant rotation, up to 130° (e.g. see 2 cases in Rust et al., 2005), with one plausible case up to 160° (Dasso et al., 2007; Harra et al., 2007). It is plausible, but not yet proven, that the largest rotations are characteristic of the kink instability, while the amount of rotation depends on the vertical gradient of the coronal field (Török, private communication).

6 Magnetic fluxes

Magnetic fluxes are not directly available from in-situ data, since the magnetic field is only measured along a line crossing the observed MC (Fig. 5). They are usually obtained by fitting a magnetic model to the data (see Dasso et al., 2005, for a review). The MC data are usually compatible with a flux rope configuration and two fluxes are deduced: axial and azimuthal. Both fluxes are sensitive to the determined orientation of the MC axis. The axial flux is specifically sensible to the unknown shape of the flux rope cross section,

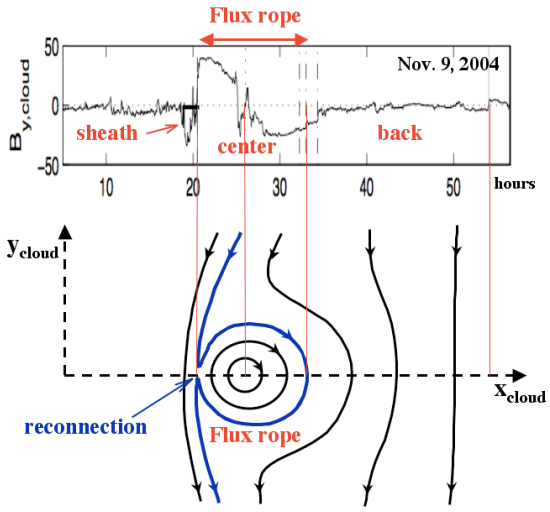

Fig. 9. Evidence of partial magnetic reconnection of a flux rope during its transit from the Sun to the spacecraft. Top panel: $By_{\rm cloud}$ field component ($\approx$ azimuthal component since the impact parameter is small) for the 9 November 2004 MC (Dasso et al., 2007). A current sheet is theoretically expected to be present between two regions with different magnetic connectivities, such as between the flux rope and its surroundings. Then, the flux rope is defined by discontinuities of $By_{\rm cloud}$ and the same azimuthal flux before and after the center ($By_{\rm cloud}$ is the dominant field component at the flux rope border). In the back of the flux rope an extended region of low but coherent field is present. This "back" region was probably belonging to the flux rope initially ejected from the Sun, but reconnection in the front with the overtaken magnetic field connected it to the solar wind (bottom panel). Then, the reconnected flux became progressively swept behind the faster flux rope. The consequence of the frontal reconnection is an extended region in the back of the MC with a weak field having low fluctuations (thus different from the solar wind field).

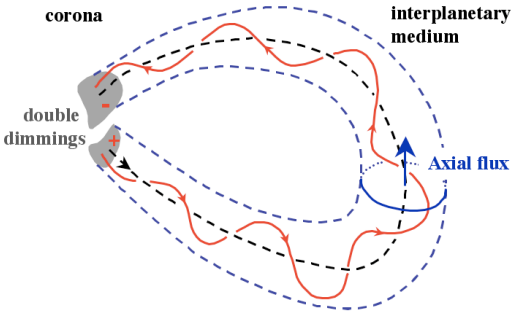

Fig. 10. Sketch showing the ejection of a flux rope already present in the corona (a negligible amount of reconnection is assumed during the ejection). When the radial extension of the field lines is well above the pressure scale height, the plasma is no longer confined in the corona by the magnetic field. It implies the formation of two dimmings at the footpoints of the flux rope. Their extension corresponds to a magnetic flux equal to the axial flux of the flux rope.

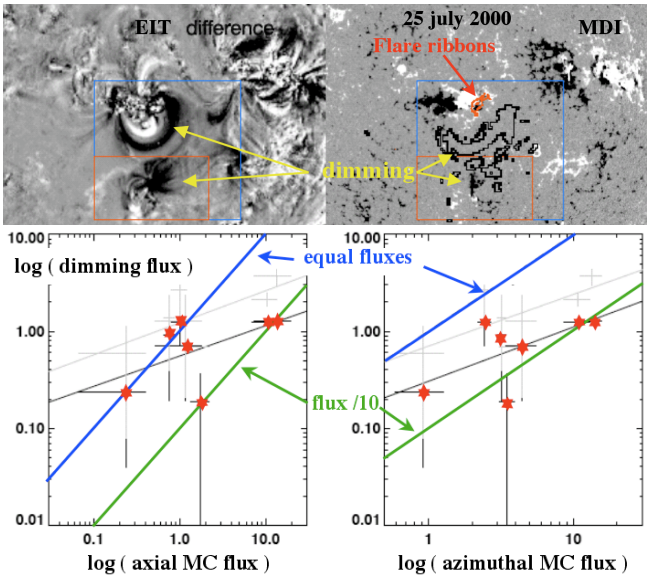

Fig. 11. Comparison of the magnetic flux found in the dimmings and in the associated MC for 7 events. The top left panel shows a base difference image for one event. The dimming extensions are reported on the co-temporal magnetogram in the right panel. The bottom panels compare the flux found in the dimmings with the axial and azimuthal flux found in the related MC. The red stars correspond to the mean of the absolute flux value between negative and positive dimming regions, and an azimuthal flux computed with MC length L=1 AU. The error bars are mainly computed from varying alignment offsets (between MDI and EIT), using two dimming levels, and using the range L=0.5 to 2 AU (Qiu et al., 2007).

while the azimuthal flux is most affected by the location of the MC boundaries, the supposed length of the flux rope, and the axial invariance hypothesis. If the spacecraft approaches the MC axis by a small fraction of its radius and with the hypothesis of cylindrical symmetry, the magnetic fluxes can also be derived directly from the data (Dasso et al., 2006). The fluxes vary by a few 10% between the different estimations.

On top of the possible flux biases shortly described above, there is the intrinsic evolution of the flux rope when moving from the Sun to the spacecraft. Flux ropes faster than the solar wind are overtaking the magnetic field usually of different orientation than their leading field, so magnetic reconnection is expected. The consequence of this reconnection, a flux tube pealed in the front but with an extended back part, was indeed found (Fig. 9). About 60% of the azimuthal flux was estimated to be lost by the MC observed on 18 October 1995 (Dasso et al., 2006). This is the maximum value detected so far. In other MCs, the reconnected flux is lower (e.g. $\approx$25% in the 9 November 2004 MC; Dasso et al., 2007), or even negligible (Mandrini et al., 2007).

In the photosphere, measurements of magnetic fluxes are classical. But the comparison to MC fluxes needs specific

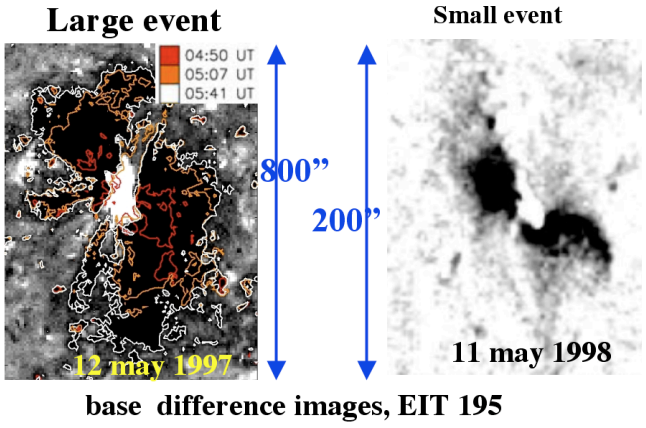

Fig. 12. Double dimmings for two eruptive events in similar bipolar magnetic fields. The large event occurred in a classical bipolar AR (Attrill et al., 2006), while the small event occurred in an ephemeral region (duration ≈2 days; Mandrini et al., 2005). The bipole and dimming magnetic fluxes are about 15 times larger in the first event than in the second. Despite this magnitude difference, these events have a similar organization both for the flare brightenings centered on the magnetic inversion line and for the dimmings shifted along it (both events have negative helicity). For the large event, the expansion evolution of the dimmings is shown. The dimming contour level is set halfway between the intensity of the quiet Sun and of a coronal hole.

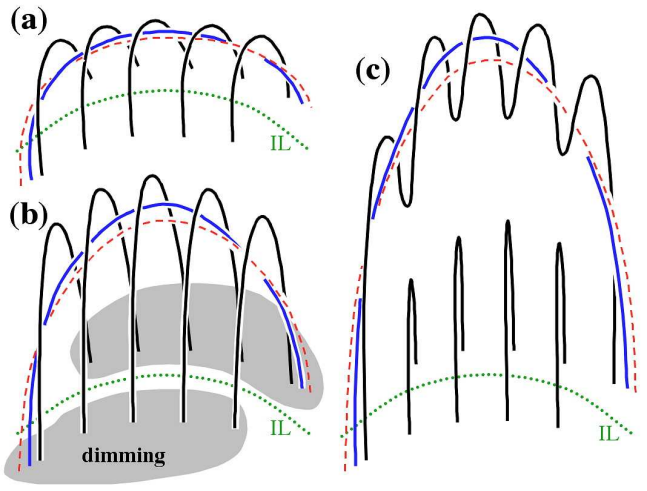

Fig. 13. A scenario for a flux rope eruption. **(a)** A flux tube (blue and red lines) is embedded in a sheared arcade (black lines). **(b)** The arcade and the flux rope expand significantly (more than the pressure scale height). Dimmings (grey areas) are formed at the footpoints of the flux rope and also of the sheared arcade. **(c)** The reconnection of the sheared arcade progressively incorporates more flux to the erupting flux tube. In this scenario the magnetic flux in each dimming corresponds to the sum of the axial and azimuthal flux in the associated MC, in contrast to the ideal case presented in Fig. 10 (Mandrini et al., 2005, 2007). The dotted green line is the magnetic photospheric inversion line (IL).

measurements, i.e. the flux involved in a CME. Extended intensity decreases in coronal images, called dimmings, are frequently observed in association with front-side CMEs (Thompson et al., 2000). The generally accepted physical interpretation of dimmings is that they are primarily a density depletion induced by the eruption of an unstable magnetic configuration (Hudson et al., 1996; Harrison and Lyons, 2000; Zarro et al., 1999). So the dimmings indicate the magnetic regions related to the associated MC.

More precisely, double dimmings are often present on both sides of the erupting configuration (Fig. 1). It has been suggested that these dimmings mark the position of the ejected flux rope footpoints (Fig. 10), since the magnetic flux found in the dimming regions corresponds approximately to the axial magnetic flux of the associated MC (Lepping et al., 1997; Webb et al., 2000; Qiu et al., 2007). Does it imply that the flux rope observed in situ was simply launch from the corona? In fact, this simple interpretation is not plausible, since MCs are highly twisted flux tubes (more than 10 turns typically; Gulisano et al., 2005) while evidence of such a high twist has never been found in the corona. A more plausible alternative would be that most of the flux rope is rapidly formed by reconnection of a sheared arcade (before the arcade height becomes larger than the plasma scale height, ≈100 Mm).

However, Mandrini et al. (2005) and Attrill et al. (2006) reached a different conclusion, as follows. They computed the magnetic flux in the dimming regions associated with eruptions occurring in two isolated bipolar ARs (Fig. 12). In both cases, they found that the flux in the dimmings was comparable mainly to the azimuthal flux of the associated MC (when assuming a length compatible with both solar and interplanetary observations). These results led these authors to propose that the ejected flux rope in these cases is mostly formed by successive reconnections in a sheared arcade during the eruption process (Fig. 13). Indeed, the formation of a twisted flux tube from a sheared arcade has been proposed by several authors either in the low corona (e.g. Amari et al., 2003), or later on (Gosling, 1990); see Forbes (2000) for a review. The initial arcade in Fig. 13 can contain an embedded flux rope. This case corresponds to the model of Lin and Forbes (2000); indeed considerable arcade field line stretching can occur before reconnection behind the flux rope and adds a significant amount of the arcade flux to the flux rope. In this model the current sheet formed behind the ascending flux rope can be as long as 3 $R_{\odot}$, while with radio imaging in the metric domain of one limb event, Pick et al. (2005) have estimated this current sheet to be not longer than one tenth of the previous value.

The above controversy on the relationship between the magnetic flux present in the dimmings and in the related MC, comes partly from the difficulties in defining the maximum extention of dimmings but also to identify the origin of

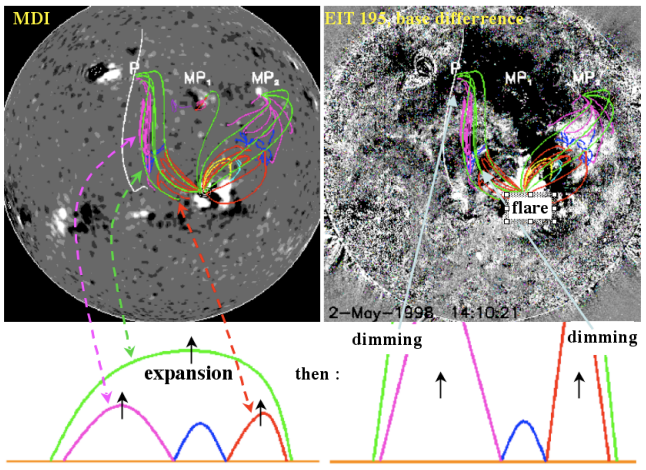

Fig. 14. Formation of large-scale dimmings by the destabilization of trans-equatorial loops. The top panels show a set of computed field lines (with a full Sun potential field extrapolation) on top of the MDI magnetogram (left panel) and a de-rotated base difference image of EIT 195 Å (right panel). The magnetic configuration involved in the eruption is quadrupolar (green, pink, blue, and red field lines). The bottom panels show a sketch for the evolution of representative field lines. Reconnection in the quadrupolar configuration provides plasma heating seen as brightenings (located near the blue field lines). The destabilization of the large field lines (green), as well as the lateral ones (pink and red), leads to the formation of large-scale dimmings (Delannée et al., 2007).

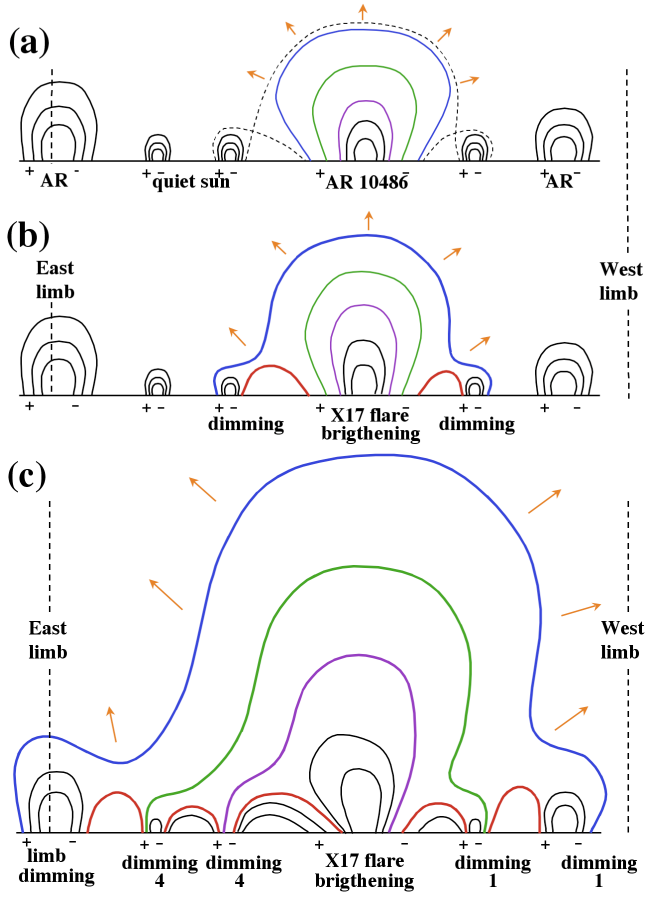

Fig. 15. Dimming spreading due to reconnection (mechanism proposed by Attrill et al., 2007, applied to the 28 October 2003 event). **(a)** The CME lift-off. AR 10486 is represented by five field lines, while nearby bipoles are represented with three black field lines. The dashed lines represent the separatrices involved in the next reconnection (drawn symmetric to simplify the drawing). **(b, c)** Reconnection of the expanding CME field configuration with the surrounding bipoles (the just reconnected field lines are thicker and set to red for the short loops). By successive reconnections the outer shell of the CME expanding magnetic field is progressively rooted in more distant regions. This creates the spreading of the dimmings to larger spatial scales (Mandrini et al., 2007).

the dimmings. In many events more than two dimmings are present and they are related to brightenings, plausibly formed by magnetic reconnection (Delannée, 2000; Delannée et al., 2007). Dimmings are also present at the footpoints of large-scale interconnecting loops (Fig. 14), plausibly destabilized during the eruption but with an unknown relationship with the associated MC. Dimmings are also spread to large distances from the initial erupting site by progressive stepping reconnection with the surrounding bipoles, making the erupting configuration large scale even in the low corona (Attrill et al., 2007). In extreme events, such as on 28 Oct. 2003, the dimmings are spread around about half the Sun. Mandrini et al. (2007) interpreted this spreading by the stepping reconnection process (Fig. 15), and they found no correspondence between the magnetic flux in the dimmings and in the related MC (this is one of the cases included in Fig. 11). Indeed, the main dimmings of the eruption are masked by the brightness of the X17 flare, while some secondary dimmings are at and behind the eastern limb. In conclusion, dimmings need to be carefully studied in each event before relating their fluxes to the associated MC fluxes.

7 Magnetic helicity

Magnetic helicity, H, quantifies how the magnetic field is sheared and twisted compared to its lowest energy state, the potential field. Such stressed magnetic fields are usually observed in association with flares, eruptive filaments, and CMEs. Magnetic helicity plays a key role in magnetohydrodynamics because it is almost preserved on a time scale less than the global diffusion time scale (which is several orders of magnitude longer than the ICME evolution time). Its conservation property permits one to achieve a quantitative link between a CME and its related MC, provided one can derive it from observations in both domains.

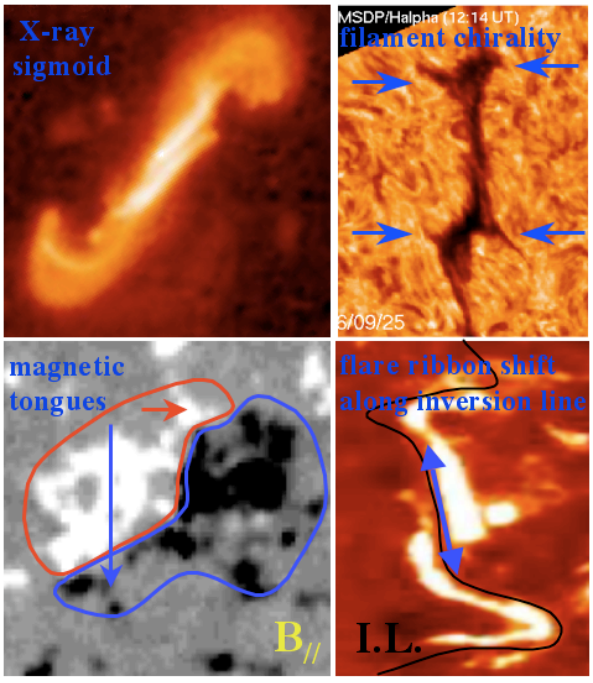

Fig. 16. Some characteristic patterns indicating a positive magnetic helicity (for negative helicity the images have to be mirrored). Soft X-ray sigmoids are the coronal trace of twisted or highly sheared field lines (Manoharan et al., 1996; Canfield et al., 1999). The global organization of fibrils and feet/barbs, i.e. their inclination on the filament axis, is another trace of a twisted/sheared magnetic field (Martin et al., 1994; Aulanier et al., 1998). The spatial distribution of the vertical magnetic field component in emerging active regions is often asymmetric, with lateral extensions to the main bipolar polarities. These "magnetic tongues" are the photospheric trace of the emerging sub-photospheric flux rope (López Fuentes et al., 2000). Finally in a sheared field, the flare ribbon locations are separated along the inversion line. In some cases, they also have a characteristic J-shape if the twist is of the order or above one turn (Démoulin et al., 1996).

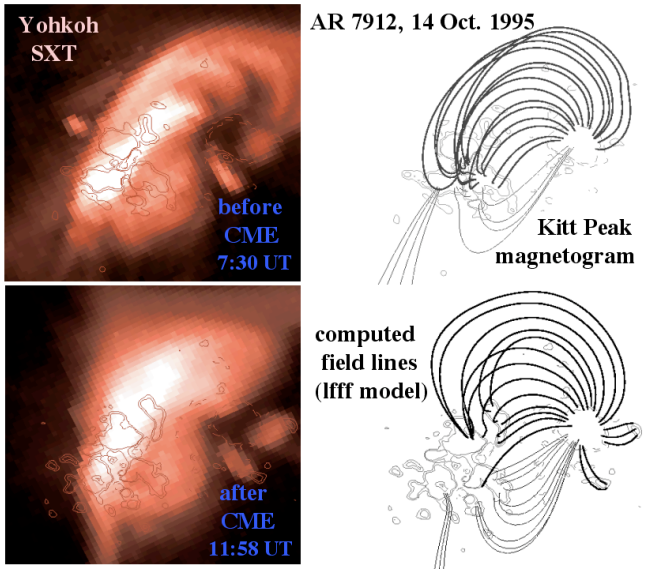

Fig. 17. Evolution of the X-ray emission and of the coronal magnetic field before and after the ejection accompanying a long duration event which is the signature of a CME. Left panels: co-aligned soft X-ray images overlaid with longitudinal magnetograms. Right panels: coronal linear force-free field models. Isocontours (±70,±140G) are drawn with continuous/dashed lines for positive/negative magnetic field values. The deduced loss of coronal magnetic helicity is comparable to the helicity found in the associated MC observed at 1 AU (Luoni et al., 2005).

The initial use of H, in linking solar to interplanetary events, involved only the sign of H (as the developments to compute its magnitude were not yet done). For MCs, the sign of H is readily obtained from the measured rotation of the vector magnetic field (without the need of a model). The most direct way to infer the sign of H in an erupting region is to analyze vector magnetograms, in particular to infer the sign of the magnetic shear (angle between the observed and the computed potential field). Also, a fit of the vector magnetic field with a linear force-free field, $\boldsymbol{j}=\alpha\boldsymbol{B}$, gives a single value, $\alpha_{\rm best}$, which represents the global shear of the region (Pevtsov et al., 1995). However, even without magnetic data, the sign of H can be frequently inferred from the "sheared orientation" of chromospheric fibrils or coronal loops (with respect to the direction given by a potential field), or by the four characteristic patterns shown in Fig. 16; see Green et al. (2007) for practical examples, and Pevtsov and Balasubramaniam (2003) for a review. It is better to use as many as possible of these patterns to infer the sign of H since fake patterns are always possible, especially in multipolar regions (e.g. a given pattern can be created by a special arrangement of magnetic polarities).

Rust (1994) and Bothmer and Schwenn (1994, 1998) found that most MCs have the same sign of H than the associated erupting filaments. They also concluded that in the Northern (resp. Southern) Hemisphere, H is preferentially negative (resp. positive), extending the results of Martin et al. (1994) obtained for quiescent filaments. These hemispherical rules are confirmed by further studies, while the importance of the dominance depends on the data set analyzed and the proxy of the helicity used (Pevtsov et al., 1995; Bao et al., 2000; Hagino and Sakurai, 2004).

The definition of H is a priori far from any data set since H involves a volume integral including the vector potential $\boldsymbol{A}$ of $\boldsymbol{B}$, or equivalently a double volume integral involving $\boldsymbol{B}$. More generally, H can be expressed in several equivalent forms, implying different types of integrals. Then, the estimation of H from data started much later than the pionnering theoretical work of Berger and Field (1984), since it was necessary to bring the theory towards the observations, in particular to find the expression of the helicity which is

best suited to include the available data. The achieved developments are reviewed by Démoulin (2007).

Magnetic helicity can be estimated by fitting a model to the MC data, just as for the estimation of magnetic fluxes (Sect. 6). Since H involves a double integral on the field, its estimation is robust, i.e. it has a low sensitivity to the model selected, provided the fit to the data is good (Dasso et al., 2003). The main limitations are due to the local nature of the data, then to the needed hypothesis on the 3-D geometry of the flux tube to compute a global quantity such as H. When the impact parameter is small, and with the hypothesis of a local cylindrical symmetry of the flux rope, H can be derived directly from the data when they are rotated in the MC frame (Dasso et al., 2006).

At the photospheric level, the rate (or flux) of magnetic helicity can be computed from the evolution of longitudinal magnetograms. Nindos et al. (2003) analyzed in detail 6 ARs producing several CMEs during their disk passage. For each AR, one CME could be associated to a MC. The helicity content of these MCs is broad: $H \approx 1$ to 19×10^{42} Mx^2 with a length estimated by the condition for the kink instability threshold (set to 2 turns). For the non-halo CMEs they used the mean helicity value derived by DeVore (2000) from a set of 18 MCs. Finally, Nindos et al. found a photospheric helicity injection broadly compatible with the ejected helicity in CMEs, both with a length set to 0.5 AU or estimated from the kink threshold.

The next step is to analyze the variation of the coronal helicity during a halo CME event, together with the associated MC. So far, this has been done only for two cases, a tiny and a large MC. Mandrini et al. (2005) analyzed the full evolution of a tiny AR well isolated from others and located close to the solar disk centre. The photospheric bipole emerged and dispersed at the photospheric level in $\approx$2 days. The variation of the coronal helicity during the eruptive event was estimated by using a linear force-free field fitted to the coronal loops. The decrease in the coronal helicity and the MC helicity were found to be in the same range: ≈ 2 to 3×10^{39} Mx^2. This value is at the lower limit of the helicity interval found in a set of 132 MCs analyzed by Lynch et al. (2005). Dasso et al. (2006) analyzed in a similar way a well studied MC, observed on 18-20 Oct. 1995. In this case the MC helicity, at least 10^{43} Mx^2, is larger by a factor of ≈ 2 than the variation of the coronal helicity in the associated CME event (Luoni et al., 2005). This factor of 2 is still small compared to the broad interval of helicities found in the MCs (factor 10^5!), so that the magnitude of the magnetic helicity is one more significant constraint in the CME/MC association.

8 Conclusions

Making a quantitative link between the CMEs and their interplanetary counterparts is an important step in understanding the physics involve. It also brings together the knowledge of two domains build on very different data. It provides important tests on the possible systematic bias present in each kind of data and their associated modeling.

The association involves a series of constraints: the relative location of the solar source and the spacecraft detecting the ICME in situ, the transit time (Sun-in situ), and the measure of the same physical parameters in both domains (orientation, magnetic fluxes and helicity). It is important to involve as many constraints as possible, in order to avoid incorrect associations (in particular when the CME rate is large, like around solar maximum).

However, if one or two constraints are not satisfied in the standard way in some event, it is worth analyzing closer this case since interesting physics is plausibly involved. For example, the CME could be deflected from a near radial propagation by the interaction with a streamer, so that the source region could be far from disk center. The transit time could be shorter than expected if the ICME is overtaken by a fast solar wind stream or another fast CME. The magnetic configuration could significantly rotate in some cases, giving a plausible signature of the kink instability. The relation between the magnetic fluxes in the dimmings and in the related MCs is still controversial. It is important to clarify this since it involves understanding not only the formation of dimmings but also the CME ejection mechanism itself and the evolution of MCs. Finally, by its conservation property, even with magnetic dissipation, magnetic helicity provides an important constraint on the global models developed from the coronal and in-situ observations.

The association CME/ICME-MC is very reliable and provides more physical information when made from different points of view, in particular when coronagraphic and in-situ observations are in quadrature (minimization of the projection effects). The two STEREO spacecraft associated with SOHO and ACE provide a unique opportunity to couple solar and interplanetary data, to further understand the physics behind the puzzling CMEs/ICMEs.

Acknowledgements. I thank S. Dasso, S. Hoang and C. H. Mandrini for their help in improving the manuscript.

Topical Editor R. Forsyth thanks X. Zhao and another anonymous referee for their help in evaluating this paper.

References

Amari, T., Luciani, J. F., Aly, J. J., Mikic, Z., and Linker, J.: Coronal mass ejection: initiation, magnetic helicity, and flux ropes. I. Boundary motion-driven evolution, Astrophys. J., 585, 1073–1086, doi:10.1086/345501, 2003.

Attrill, G., Nakwacki, M. S., Harra, L. K., et al.: Using the evolution of coronal dimming regions to probe the global magnetic field topology, Solar Phys., 238, 117–139, doi:10.1007/s11207-006-0167-5, 2006.

Attrill, G., Harra, L. K., van Driel-Gesztelyi, L., and Démoulin, P.: Coronal "wave": magnetic footprint of a CME?, Astrophys. J. Lett., 656, L101–L104, 2007.

Aulanier, G., Démoulin, P., van Driel-Gesztelyi, L., Mein, P., and Deforest, C.: 3-D magnetic configurations supporting prominences. II. The lateral feet as a perturbation of a twisted flux-tube, Astron. Astrophys., 335, 309–322, 1998.

Aulanier, G., Démoulin, P., and Grappin, R.: Equilibrium and observational properties of line-tied twisted flux tubes, Astron. Astrophys., 430, 1067–1087, doi:10.1051/0004-6361:20041519, 2005.

Bao, S. D., Pevtsov, A. A., Wang, T. J., and Zhang, H. Q.: Helicity computation using observations from two different polarimetric instruments, Solar Phys., 195, 75–87, 2000.

Berdichevsky, D. B., Farrugia, C. J., Thompson, B. J., et al.: Halo-coronal mass ejections near the 23rd solar minimum: lift-off, inner heliosphere, and in situ (1 AU) signatures, Annales Geophysicae, 20, 891–916, 2002.

Berger, M. A. and Field, G. B.: The topological properties of magnetic helicity, J. Fluid. Mech., 147, 133–148, 1984.

Bothmer, V. and Schwenn, R.: Eruptive prominences as sources of magnetic clouds in the solar wind, Space Science Rev., 70, 215–220, 1994.

Bothmer, V. and Schwenn, R.: The structure and origin of magnetic clouds in the solar wind, Annales Geophysicae, 16, 1–24, 1998.

Burlaga, L. F.: Interplanetary magnetohydrodynamics, New York : Oxford University Press, 1995.

Burlaga, L. F., Klein, L., Sheeley, Jr., N. R., et al.: A magnetic cloud and a coronal mass ejection, Geophys. Res. Lett., 9, 1317–1320, 1982.

Canfield, R. C., Hudson, H. S., and McKenzie, D. E.: Sigmoidal morphology and eruptive solar activity, Geophys. Res. Lett., 26, 627–630, doi:10.1029/1999GL900105, 1999.

Dasso, S., Mandrini, C. H., Démoulin, P., and Farrugia, C. J.: Magnetic helicity analysis of an interplanetary twisted flux tube, J. Geophys. Res., 108, 1362, doi:10.1029/2003JA009942, 2003.

Dasso, S., Mandrini, C. H., Démoulin, P., Luoni, M. L., and Gulisano, A. M.: Large scale MHD properties of interplanetary magnetic clouds, Adv. Space Res., 35, 711–724, doi:10.1016/j.asr.2005.02.096, 2005.

Dasso, S., Mandrini, C. H., Démoulin, P., and Luoni, M. L.: A new model-independent method to compute magnetic helicity in magnetic clouds, Astron. Astrophys., 455, 349–359, doi:10.1051/0004-6361:20064806, 2006.

Dasso, S., Nakwacki, M. S., Démoulin, P., and Mandrini, C. H.: Progressive transformation of a flux rope to an ICME, Solar Phys., 244, 115–137, doi:10.1007/s11207-007-9034-2, 2007.

Delannée, C.: Another view of the EIT wave phenomena, Astrophys. J., 545, 512–523, 2000.

Delannée, C., Hochedez, J.-F., and Aulanier, G.: Stationary parts of an EIT and Moreton wave: a topological model, Astron. Astrophys., 465, 603–612, doi:10.1051/0004-6361:20065845, 2007.

Démoulin, P.: Recent theoretical and observational developments in magnetic helicity studies, Adv. Space Res., 39, 1674–1693, 2007.

Démoulin, P., Priest, E. R., and Lonie, D. P.: Three-dimensional magnetic reconnection without null points 2. Application to twisted flux tubes, J. Geophys. Res., 101, 7631–7646, doi:10.1029/95JA03558, 1996.

DeVore, C. R.: Magnetic helicity generation by solar differential rotation, Astrophys. J., 539, 944–953, 2000.

Forbes, T. G.: A review on the genesis of coronal mass ejections, J. Geophys. Res., 105, 23 153–23 166, 2000.

Funsten, H. O., Gosling, J. T., Riley, P., et al.: Combined Ulysses solar wind and SOHO coronal observations of several west limb coronal mass ejections, J. Geophys. Res., 104, 6679–6690, doi:10.1029/1998JA900088, 1999.

Gibson, S. E., Fan, Y., Mandrini, C., Fisher, G., and Démoulin, P.: Observational consequences of a magnetic flux rope emerging into the corona, Astrophys. J., 617, 600–613, doi:10.1086/425294, 2004.

Gopalswamy, N., Lara, A., Lepping, R. P., et al.: Interplanetary acceleration of coronal mass ejections, Geophys. Res. Lett., 27, 145–148, 2000.

Gopalswamy, N., Lara, A., Yashiro, S., Kaiser, M. L., and Howard, R. A.: Predicting the 1-AU arrival times of coronal mass ejections, J. Geophys. Res., 106, 29 207–29 218, doi:10.1029/2001JA000177, 2001.

Gosling, J. T.: Coronal mass ejections and magnetic flux ropes in interplanetary space, Washington DC American Geophysical Union Geophysical Monograph Series, 58, 343–364, 1990.

Green, L. M., Kliem, B., Török, T., van Driel-Gesztelyi, L., and Attrill, G. D. R.: Transient coronal sigmoids and rotating erupting flux ropes, Solar Phys., 246, 365–392, 2007.

Gulisano, A. M., Dasso, S., Mandrini, C. H., and Démoulin, P.: Magnetic clouds: A statistical study of magnetic helicity, J. Atmos. Solar-Terr. Phys., 67, 17–18, 2005.

Gulisano, A. M., Dasso, S., Mandrini, C. H., and Démoulin, P.: Estimation of the bias of the minimum variance technique in the determination of magnetic clouds global quantities and orientation, Adv. Space Res., (ISSN 0273-1177), 40, 1881–1890, 2007.

Hagino, M. and Sakurai, T.: Latitude variation of helicity in solar active regions, Publ. Astron. Soc. Japan, 56, 831–843, 2004.

Harra, L. K., Crooker, N. U., Mandrini, C. H., et al.: How does large flaring activity from the same active region produce oppositely directed magnetic louds?, Solar Phys., 244, 95–114, doi:10.1007/s11207-007-9002-x, 2007.

Harrison, R. A. and Lyons, M.: A spectroscopic study of coronal dimming associated with a coronal mass ejection, Astron. Astrophys., 358, 1097–1108, 2000.

Hoang, S., Lacombe, C., MacDowall, R. J., and Thejappa, G.: Radio tracking of the interplanetary coronal mass ejection driven shock crossed by Ulysses on 10 May 2001, J. Geophys. Res., 112, A09102, doi:10.1029/2006JA011906, 2007.

Hudson, H. S., Acton, L. W., and Freeland, S. L.: A long-duration solar flare with mass ejection and global consequences, Astrophys. J., 470, 629–635, doi:10.1086/177894, 1996.

Jian, L., Russell, C. T., Luhmann, J. G., and Skoug, R. M.: Properties of interplanetary coronal mass ejections at one AU during 1995 - 2004, Solar Phys., 239, 393–436, doi:10.1007/s11207-006-0133-2, 2006.

Lepping, R. P., Szabo, A., DeForest, C. E., and Thompson, B. J.: Magnetic flux in modeled magnetic clouds at 1 AU and some specific comparisons to associated photospheric flux, in: ESA SP-415: Correlated Phenomena at the Sun, in the Heliosphere and in Geospace, edited by: Wilson, A., 163–170, 1997.

Lin, J. and Forbes, T. G.: Effects of reconnection on the coronal mass ejection process, J. Geophys. Res., 105, 2375–2392, 2000.

Lindsay, G. M., Luhmann, J. G., Russell, C. T., and Gosling, J. T.: Relationships between coronal mass ejection speeds from coronagraph images and interplanetary characteristics of associated

interplanetary coronal mass ejections, J. Geophys. Res., 104, 12 515–12 524, doi:10.1029/1999JA900051, 1999.

López Fuentes, M. C., Démoulin, P., Mandrini, C. H., and van Driel-Gesztelyi, L.: The counterkink rotation of a non-Hale active region, Astrophys. J., 544, 540–549, doi:10.1086/317180, 2000.

Luoni, M. L., Mandrini, C. H., Dasso, S., van Driel-Gesztelyi, L., and Démoulin, P.: Tracing magnetic helicity from the solar corona to the interplanetary space, J. Atmos. Solar-Terr. Phys., 67, 1734–1743, doi:10.1016/j.jastp.2005.07.003, 2005.

Lynch, B. J., Gruesbeck, J. R., Zurbuchen, T. H., and Antiochos, S. K.: Solar cycle-dependent helicity transport by magnetic clouds, J. Geophys. Res., 110, A08107, doi:10.1029/2005JA011137, 2005.

Mandrini, C. H., Pohjolainen, S., Dasso, S., et al.: Interplanetary flux rope ejected from an X-ray bright point. The smallest magnetic cloud source-region ever observed, Astron. Astrophys., 434, 725–740, doi:10.1051/0004-6361:20041079, 2005.

Mandrini, C. H., Nakwacki, M. S., Attrill, G., et al.: Are CME-related dimmings always a simple signature of interplanetary magnetic cloud footpoints?, Solar Phys., 244, 25–43, doi:10.1007/s11207-007-9020-8, 2007.

Manoharan, P. K., van Driel-Gesztelyi, L., Pick, M., and Démoulin, P.: Evidence for large-scale solar magnetic reconnection from radio and X-ray measurements, Astrophys. J. Lett., 468, L73–L77, 1996.

Martin, S. F., Bilimoria, R., and Tracadas, P. W.: Magnetic field configurations basic to filament channels and filaments, in: Solar Surface Magnetism, edited by Rutten, R. J. and Schrijver, C. J., p. 303, 1994.

Marubashi, K.: Interplanetary magnetic flux ropes and solar filaments, in: Coronal Mass Ejections, Geophysical Monograph 99, 147–156, 1997.

Michałek, G., Gopalswamy, N., Lara, A., and Manoharan, P. K.: Arrival time of halo coronal mass ejections in the vicinity of the Earth, Astron. Astrophys., 423, 729–736, doi:10.1051/0004-6361:20047184, 2004.

Nindos, A., Zhang, J., and Zhang, H.: The magnetic helicity budget of solar active regions and coronal mass ejections, Astrophys. J., 594, 1033–1048, 2003.

Pevtsov, A. A. and Balasubramaniam, K. S.: Helicity patterns on the sun, Adv. Space Res., 32, 1867–1874, 2003.

Pevtsov, A. A., Canfield, R. C., and Metcalf, T. R.: Latitudinal variation of helicity of photospheric magnetic fields, Astrophys. J. Lett., 440, L109–L112, doi:10.1086/187773, 1995.

Pick, M., Démoulin, P., Krucker, S., Malandraki, O., and Maia, D.: Radio and X-ray signatures of magnetic reconnection behind an ejected flux rope, Astrophys. J., 625, 1019–1026, doi:10.1086/429530, 2005.

Qiu, J., Hu, Q., Howard, T. A., and Yurchyshyn, V. B.: On the magnetic flux budget in low-corona magnetic reconnection and interplanetary coronal mass ejections, Astrophys. J., 659, 758–772, doi:10.1086/512060, 2007.

Reiner, M. J., Kaiser, M. L., Fainberg, J., and Stone, R. G.: A new method for studying remote type II radio emissions from coronal mass ejection-driven shocks, J. Geophys. Res., 103, 29 651–29 664, 1998.

Reiner, M. J., Kaiser, M. L., and Bougeret, J.-L.: Coronal and interplanetary propagation of CME/shocks from radio, in situ and white-light observations, Astrophys. J., 663, 1369–1385, doi:10.1086/518683, 2007.

Rust, D. M.: Spawning and shedding helical magnetic fields in the solar atmosphere, Geophys. Res. Lett., 21, 241–244, 1994.

Rust, D. M., Anderson, B. J., Andrews, M. D., et al.: Comparison of interplanetary disturbances at the NEAR spacecraft with coronal mass ejections at the Sun, Astrophys. J., 621, 524–536, doi:10.1086/427401, 2005.

Ruzmaikin, A., Martin, S., and Hu, Q.: Signs of magnetic helicity in interplanetary coronal mass ejections and associated prominences: Case study, J. Geophys. Res., 108, 1096, doi:10.1029/2002JA009588, 2003.

Schwenn, R., Dal Lago, A., Huttunen, E., and Gonzalez, W. D.: The association of coronal mass ejections with their effects near the Earth, Annales Geophysicae, 23, 1033–1059, 2005.

St. Cyr, O. C., Howard, R. A., Sheeley, N. R. J., et al.: Properties of coronal mass ejections: SOHO LASCO observations from January 1996 to June 1998, J. Geophys. Res., 105(A8), 18 169–18 186, doi:10.1029/1999JA000381, 2000.

Thernisien, A. F. R., Howard, R. A., and Vourlidas, A.: Modeling of flux rope coronal mass ejections, Astrophys. J., 652, 763–773, 2006.

Thompson, B. J., Cliver, E. W., Nitta, N., Delannée, C., and Delaboudinière, J.-P.: Coronal dimmings and energetic CMEs in April-May 1998, Geophys. Res. Lett., 27, 1431–1434, doi:10.1029/1999GL003668, 2000.

Török, T. and Kliem, B.: The evolution of twisting coronal magnetic flux tubes, Astron. Astrophys., 406, 1043–1059, 2003.

Török, T. and Kliem, B.: Confined and ejective eruptions of kink-unstable flux ropes, Astrophys. J. Lett., 630, L97–L100, doi:10.1086/462412, 2005.

Watari, S., Watanabe, T., and Marubashi, K.: Soft X-ray solar activities associated with interplanetary magnetic flux ropes, Solar Phys., 202, 363–384, 2001.

Webb, D. F., Lepping, R. P., Burlaga, L. F., et al.: The origin and development of the May 1997 magnetic cloud, J. Geophys. Res., 105, 27 251–27 260, doi:10.1029/2000JA000021, 2000.

Weiss, L. A., Gosling, J. T., McAllister, A. H., et al.: A comparison of interplanetary coronal mass ejections at ULYSSES with YOHKOH soft X-ray coronal events, Astron. Astrophys., 316, 384–395, 1996.

Yurchyshyn, V., Hu, Q., and Abramenko, V.: Structure of magnetic fields in NOAA active regions 0486 and 0501 and in the associated interplanetary ejecta, Space Weather, 3, S08C02, doi:10.1029/2004SW000124, 2005.

Yurchyshyn, V., Liu, C., Abramenko, V., and Krall, J.: The May 13, 2005 eruption: observations, data analysis and interpretation, Solar Phys., 239, 317–335, doi:10.1007/s11207-006-0177-3, 2006.

Yurchyshyn, V. B., Wang, H., Goode, P. R., and Deng, Y.: Orientation of the magnetic fields in interplanetary flux ropes and solar filaments, Astrophys. J., 563, 381–388, 2001.

Zarro, D. M., Sterling, A. C., Thompson, B. J., Hudson, H. S., and Nitta, N.: SOHO EIT observations of extreme-ultraviolet "dimming" associated with a halo coronal mass ejection, Astrophys. J. Lett., 520, L139–L142, doi:10.1086/312150, 1999.

Zhang, H.-Q., Bao, X.-M., Zhang, Y., et al.: Three super active regions in the descending phase of solar cycle 23, Chinese J. Astron. Astrophys., 3, 491–494, 2003.

Zhao, X. P.: Inversion solution of the elliptic cone model for disk

frontside full halo coronal mass ejection, J. Geophys. Res., in press, 2007.

Zhao, X. P. and Hoeksema, J. T.: Central axial field direction in magnetic clouds and its relation to southward interplanetary magnetic field events and dependence on disappearing solar filaments, J. Geophys. Res., 103, 2077–2083, 1998.

Zhukov, A. N. and Veselovsky, I. S.: Global coronal mass ejections, Astrophys. J. Lett., 664, 131–134, 2007.